

APCAT A2364

Catalyst dispersion on supported ultramicroporous inorganic membranes using derivatized silylation agents

N.K. Raman and T.L. Ward

The UNM/NSF Center for Microengineered Ceramics, University of New Mexico, Albuquerque, NM 87131 (USA)

C.J. Brinker

*The UNM/NSF Center for Microengineered Ceramics, University of New Mexico, Albuquerque, NM 87131 (USA) and
Ceramic Synthesis and Inorganic Chemistry Department 1846, Sandia National Laboratories, Albuquerque, NM 87185 (USA)*

R. Sehgal, D.M. Smith, Z. Duan and M. Hampden-Smith

The UNM/NSF Center for Microengineered Ceramics, University of New Mexico, Albuquerque, NM 87131 (USA)

and

J.K. Bailey and T.J. Headley

Ceramic Synthesis and Inorganic Chemistry Department 1846, Sandia National Laboratories, Albuquerque, NM 87185 (USA)

(Received 30 May 1992, revised manuscript received 11 August 1992)

Abstract

Two approaches were utilized to disperse rhodium metal particles onto the ultramicroporous silica separation layer of a composite inorganic membrane prepared by modification of a commercial alumina support. In one approach, the silica membrane surface was first amine-derivatized using the silylation agent $\text{H}_2\text{N}(\text{CH}_2)_2\text{NH}(\text{CH}_2)_3\text{Si}(\text{OCH}_3)_3$, followed by reaction with the metal-organic compound [(1,5-COD) RhCl] $_2$. This approach led to uniformly dispersed ca. 6 nm rhodium particles located only on the surface of the membrane (as revealed by cross-sectional transmission electron microscopy) after a hydrogen reduction at 200°C. The size of the [(1,5-COD) RhCl] $_2$ molecule combined with a reduction of the pore size due to silylation apparently prevented significant penetration into the membrane separation layer. Modest reductions (ca. 50%) in helium and nitrogen permeability resulted from this treatment. An alternative procedure involved wet impregnation of the membrane with a $\text{Rh}(\text{acac})_3$ /THF solution, followed by air calcination and hydrogen reduction. This approach produced a much lower coverage of ca. 4 nm rhodium particles. Helium and nitrogen permeability measurements indicated that considerable pore blockage existed after the calcination step, and that the reduction step led to defect

Correspondence to: Dr. C.J. Brinker, Ceramic Synthesis and Inorganic Chemistry Department 1846, Sandia National Laboratories, Albuquerque, NM 87185, USA. Tel. (+1-505)8458930, fax. (+1-505)8442974

or crack formation in the SiO₂ membrane layer as evidenced by a sizeable increase in permeability. It was proposed that the silylation approach led to the [(1,5-COD) RhCl]₂ precursor being located primarily on the surface with little pore penetration, while the Rh(acac)₃ was able to penetrate the pores to a greater extent, leading to damage of the membrane layer during decomposition of the ligands. The silylation approach appears to be a general strategy to control the size, surface coverage, and location of catalyst in catalytic membrane design.

Keywords: catalyst dispersion; composites; membranes; membrane reactor; rhodium; silylation

INTRODUCTION

There is currently a great deal of interest in using inorganic membrane reactors for selective catalytic synthesis of industrial chemicals [1]. This interest stems largely from the substantial plant capital and operational savings that can be realized by reduction of throughput if conversion efficiencies or selectivities can be increased. The concept of shifting the thermodynamic equilibrium in reversible reactions by selective removal of one of the products provides the possibility of achieving greater conversion at a lower operating temperature [2,3]. Membrane reactors can also improve reaction selectivity by suppressing side reactions that depend on product concentration [4].

A catalyst can be incorporated into a membrane reactor in several ways: (1) the membrane material itself may be catalytically active, (2) the membrane may be coated or impregnated with the catalyst, or (3) the catalyst may be present as a bed of particles contained by the membrane [5,6]. The majority of modelling and experimental studies have evaluated the configuration involving a catalyst bed contained by the membrane, and this configuration has been shown to be capable of providing considerable conversion enhancements [5,6]. There have also been studies which indicate that, under some conditions with gaseous and gas-liquid reactions, incorporation of the catalyst into the membrane itself can provide superior performance compared to configurations where the catalyst and membrane are separated [3,7,8].

There are several potential advantages to the catalytic membrane configuration. By providing the reaction product separation within the reaction zone (as opposed to at the boundaries of the reaction zone as is done with a packed catalyst bed), the transport restrictions associated with transporting the products out of the catalyst bed to the membrane are avoided. In addition, for reactions involving two separate reactant streams (e.g. multiphase reactions [7]), there may be advantages to controlling the catalyst-reactant contact precisely by permeating reactants from opposite sides of membrane and having the catalyst located as a film on one side of the membrane. An example of this for gas-liquid reactions was discussed by Harold [7]; and an important example involving gaseous reaction is the partial oxidation or oxidative coupling of methane, where selectivity and conversion are sensitive to the rate and chem-

ical form of oxygen delivery [9,10]. The primary potential disadvantages of the catalytic membrane configuration are the relatively limited area for catalyst dispersion, which may limit the catalyst loading and catalytic surface area, and limited contact time between reactants in the catalytic reaction zone.

An attractive scheme for fabricating catalytic membranes should, therefore, have several features. A high catalytic surface area should be achieved on or within the membrane without substantially hindering the permeability of the membrane. A high catalyst surface area can be best achieved with minimal catalyst loading by providing a very fine and uniform dispersion of catalyst particles. It is also important that heat treatments required to disperse and activate the catalyst do not alter the membrane microstructure. A catalyst dispersion technique which requires low temperatures to provide the active catalyst is thus desirable both with respect to impact on the membrane support and minimizing catalyst particle growth. Particle size of the catalyst and particle/support interactions are also known to influence the kinetics and the selectivity of reactions. Thus, the location and dispersion of a catalyst (e.g. within pores or on the surface of the membrane) are factors that are likely to impact performance of a membrane reactor.

There have been several reported studies of ceramic membrane reactors involving catalyst dispersion or impregnation in the membrane [3,8,11-15]. These have included wet impregnation of iron, potassium, aluminum, and copper from nitrate solutions [11]; impregnation of platinum in porous vycor from chloroplatinic acid solution [3,12]; impregnation of silver and MgO from nitrate, acetate, or nitrate/urea solutions [8,13,14]; and impregnation of vanadia from a toluene solution of vanadium acetylacetonate (acac) [15]. The use of solution impregnation followed by heat treatment has led to negligible change in permeability in some cases (e.g. platinum impregnation of porous vycor using chloroplatinic acid [12]), but may also lead to very large reductions in permeability due to pore plugging, as witnessed with impregnation of several metal nitrates in porous alumina membranes [11]. In general, the effects of impregnation techniques on the permeabilities and catalyst dispersion, loading, and particle size in membranes have not been thoroughly investigated and are not well understood.

An alternative approach to achieve highly dispersed catalyst within a porous matrix involves utilizing chemical interactions between the membrane surface (or modified membrane surface) and the metal precursor molecules. For example, it has been proposed that some metal (acac) compounds react with hydroxyl groups of oxide supports which may lead to monolayer coverage of a catalyst material [16]. Vanadium (acac) was used as a precursor to give a vanadia loading of ca. 70% of a monolayer on a porous TiO₂ membrane. [15]. Such a molecular-level dispersion approach should be very attractive and offer high activity per amount of catalyst loading if particle coarsening and damage of the membrane can be avoided in calcination and catalyst activation treatments.

Two approaches to catalyst dispersion on ceramic membrane supports are considered in this paper. One is a wet impregnation using a $\text{Rh}(\text{acac})_3$ /tetrahydrofuran (THF) solution. The second approach is based on the reaction of metal-organic precursors with an amine derivatized ultramicroporous silicate membrane layer deposited on a commercial alumina membrane. Amine derivatization of either silicon alkoxides or high surface area silica gels has been used to create metal complexation sites that provide, after reaction with metal precursors, calcination, and reduction, nanometer-sized metal particles highly dispersed within a silica matrix [17,18]. With this approach metal-organic molecules are used as reagents for site specific surface reactions leading to dispersion of the metal-organic complex at the molecular level. The dispersion is ultimately controlled by the number and distribution of the amine complexing sites which depend in turn on the number and distribution of surface hydroxyl groups and steric constraints imposed by the pore size. The metal-organic reagents may be reacted with the derivatized silicon alkoxides prior to or during sol-gel condensation reactions [18], or may be reacted in a subsequent step with an amine-derivatized silica [17]. For example, Rousseau et al. [17] reacted functionalized silicates, $[\text{H}_2\text{N}(\text{CH}_2)_2\text{N}(\text{CH}_2)_3\text{SiO}_{1.5}]_n$ with $(\text{NBD})\text{RhCl}_2$ (where NBD = norbornadiene) to obtain a homogeneous distribution of ca. 4 nm rhodium particles throughout the silica matrix. Silylation also provides a general approach for altering pore size and surface chemistry within membrane pores [19].

EXPERIMENTAL

Sol preparation and characterization

The model silica membranes used in this study were prepared by the deposition of polymeric silicate sols. The silicate sols were synthesized from tetraethoxysilane (TEOS) dissolved in ethanol using a two-step acid-catalyzed hydrolysis procedure (A2) [20]. In the first step TEOS, ethanol, water, and HCl were combined in the molar ratios: 1.0:3.8:1.0: $7.0 \cdot 10^{-4}$ and refluxed at 60°C for 90 min. In the second step additional acid and water were added at room temperature resulting in the final molar ratios (TEOS: $\text{CH}_3\text{CH}_2\text{OH}$: H_2O :HCl): 1.0:3.8:5.1:0.06. The sols were allowed to age at 50°C for a period of 10 h to promote polymerization as monitored by small angle X-ray scattering (SAXS) [21], and then diluted 2:1 with ethanol (volume ethanol:volume sol). A schematic of our experimental procedure is presented in Fig. 1.

Sol deposition

Membranes were fabricated by casting/dip coating the sol onto the inner surface of a tubular alumina support supplied by Alcoa (now supplied by U.S.

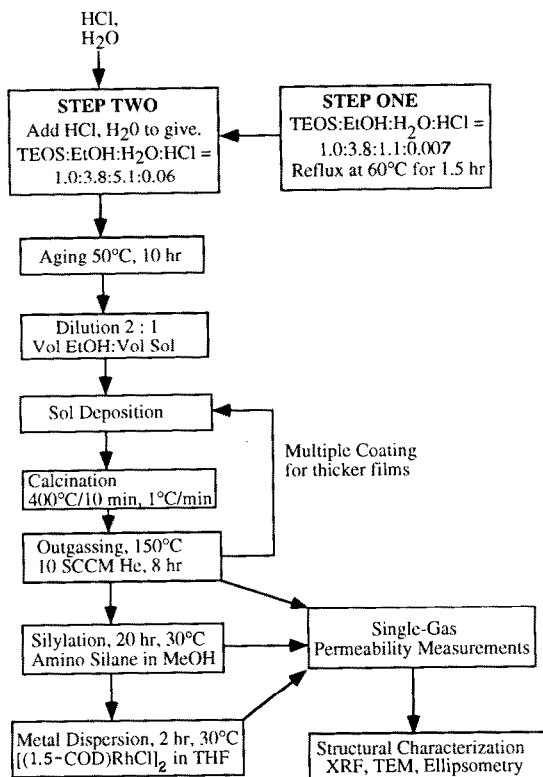


Fig. 1. Schematic of the sol and membrane preparation and characterization.

Filter) with a nominal pore diameter of 40 Å. Short sections of the tube of approximately 5 cm length were cut with a diamond wafering saw, cleaned with carbon dioxide “snow”, and outgassed in helium at 150 °C for 8 h prior to membrane deposition. The outgassed tubes were then mounted on a linear translation stage in a dry box and dipped into the sol at a rate of 20 cm/min. The contact time between the sol and the support was kept at 100 s for all the samples unless otherwise stated. The tubes were then withdrawn at a rate of 20 cm/min and allowed to dry in a flowing nitrogen ambient for 15 min. Companion thin film samples were deposited from the same sol on solid <100> single crystal silicon wafers for ellipsometric measurements [21]. The deposited membranes and films were calcined in air at a rate of 1 °C/min to 400 °C, soaked at 400 °C for 10 min, and cooled to room temperature. Thicker membranes were prepared by carrying out several dipping and calcination steps.

Silylation reaction

Surface silylation comprised reaction of the membrane surface silanol groups with an amine-derivatized silylation agent, *N*-(2-aminoethyl)-3-aminopro-

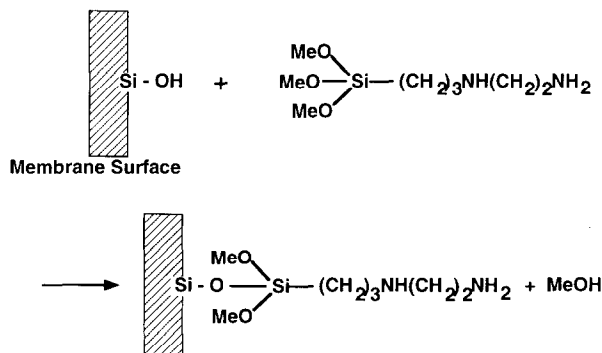


Fig. 2. Schematic representation of the silylation reaction on the membrane surface.

pyltrimethoxysilane ($H_2N(CH_2)_2NH(CH_2)_3Si(OCH_3)_3$), as shown in Fig. 2. In a typical experiment, the calcined membrane surfaces were reacted with 100 ml of methanol containing 2.2 g of $H_2N(CH_2)_2NH(CH_2)_3Si(OCH_3)_3$ with rapid stirring for 20 h at room temperature. The tubes were then washed in methanol for 1 h and dried at 100–115°C for 1 h. The amount of silylating agent used was in large excess of the stoichiometric amount needed for the complete reaction of the hydroxyl groups, assuming a surface coverage of hydroxyl groups of 4.6 OH/nm², a membrane surface area of 800 m²/gm (typical values for an A2 xerogel) [20], and a membrane thickness of 1000 Å (based on X-ray fluorescence and transmission electron microscopy measurements [21]).

Metal dispersion

Two approaches were taken to disperse rhodium in the ceramic membranes. In one approach, amine derivatized membranes (prepared by silylation as described above) were reacted with [(1,5-COD) RhCl]₂ (where (1,5-COD) is 1,5-cyclooctadiene) to produce a molecular dispersion of metal on the surface of the membrane as depicted schematically in Fig. 3. This reaction stoichiometry is based on model experiments using tetramethylethylenediamine, TMEDA, where the product (1,5-COD)ClRhN(CH₃)₂(CH₂)₂N(CH₃)₂Rh(1,5-COD)Cl is formed. The rationale for the choice of [(1,5-COD) RhCl]₂ as a source of rhodium metal is based on the observation that Rh^I compounds are easily reduced to form Rh⁰ metal, and that nanometer-sized metal rhodium crystallites can be formed. Furthermore, studies of the reaction of [(1,5-COD) RhCl]₂ with TMEDA reveal that 1,5-COD ligands remain intact to form [(1,5-COD) RhCl]₂TMEDA with the structure analogous to that proposed in Fig. 3 based on multinuclear solution nuclear magnetic resonance (NMR) experiments. The thermal decomposition of [(1,5-COD) RhCl]₂TMEDA was stud-

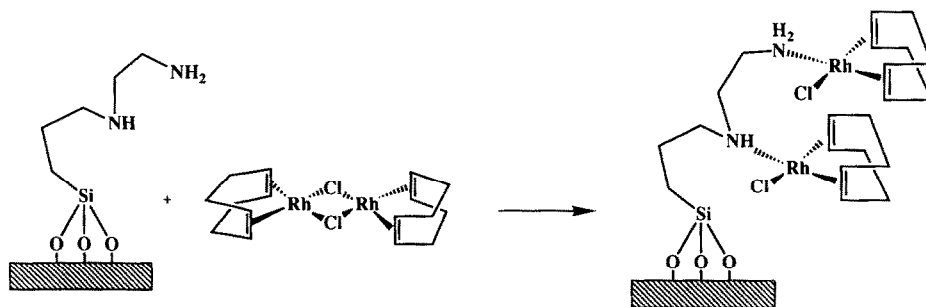


Fig. 3. Depiction of hypothesized mechanism for complexation of the $[(1,5\text{-COD})\text{RhCl}]_2$ precursor with the silylated surface.

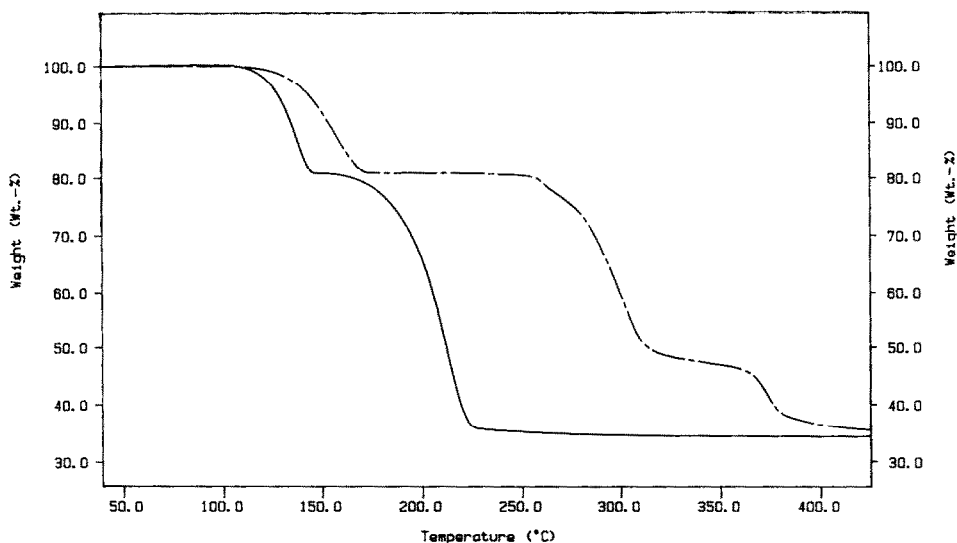


Fig. 4. Thermogravimetric analysis data for $[(1,5\text{-COD})\text{RhCl}]_2$ TMEDA under (a) air ambient (dashed line) and (b) 7% hydrogen in nitrogen atmosphere (solid line) showing the difference in thermal decomposition behavior.

ied under a number of different conditions. Thermogravimetric analysis (TGA) studies in air (see Fig. 4) revealed mass changes that correspond to the following transformations: (1) loss of TMEDA (ca. 120–175°C), (2) loss of 1,5-COD (ca. 270–310°C), (3) loss of Cl (ca. 360–375°C) to form Rh^0 , and finally oxidation at ca. 550°C to form Rh_2O_3 . The formation of crystalline Rh^0 and Rh_2O_3 were confirmed by X-ray diffraction (XRD).

The formation of Rh^0 under these conditions is close to conditions where there may be concerns about thermal stability of some ceramic membrane materials. Thermal decomposition under hydrogen occurred under much milder conditions. A weight change consistent with the loss of TMEDA was observed

first (ca. 120–140°C) analogous to the sample heated in air. However, in a hydrogen atmosphere this was immediately followed by the loss of 1,5-COD and Cl to form Rh⁰ metal by ca. 220°C (see Fig. 4). As a result of these experiments, the thermal decomposition of the amine-complexed [(1,5-COD) RhCl]₂ in the membrane was carried out at 200–220°C under a hydrogen atmosphere.

The reaction with [(1,5-COD) RhCl]₂ was conducted in the following manner. The silylated membrane tube was mounted in a Teflon coating cell which enabled the inside of the tube to be filled (keeping the outside dry) with a solution of tetrahydrofuran (THF) containing about 100 mg of [(1,5-COD) RhCl]₂ compound. The reaction was carried out for 2 h at 30°C. The tubes were then washed in THF for about 30 min and reduced in a tube furnace at 200–225°C with hydrogen flowing at 15–20 cm³/min for about 2 h to form dispersed metal crystallites.

The second approach that was utilized involved wet impregnation of the non-silylated silica membrane layer with a rhodium(III) acetylacetonate (Rh(acac)₃) solution. After formation of the membrane layer as described above, the tube was mounted in the Teflon cell and the inside surface was contacted with a Rh(acac)₃ solution (100 mg of Rh(acac)₃ dissolved in 25 ml of THF) for a period of 1 h at 25°C. The membrane tube was then washed in THF by soaking for 30 min, calcined in air at 200°C for 2 h (ramp rate of 2°C/min), and reduced in flowing hydrogen for 2 h at 200°C. The rationale behind this approach was to use a commonly encountered organometallic which could be deposited using similar solvents and washes, and might have some direct chemical interaction with the membrane support [16] without utilizing the silylation treatment, thus providing a basis for comparison for the other technique.

Structural characterization of membranes

X-ray fluorescence

Broken fragments of the coated supports were examined by a micro X-ray fluorescence method (Fisons/KeveX Omicron EDS Analyzer) to determine the areal averaged content of the composite membrane/support structure. Micro-spot analysis was used to avoid errors due to curvature effects. Silicon content per unit area was converted to thickness by assuming all the silicon was contained in a discrete silicate layer of density 2.0 g/cm³.

Transmission electron microscopy (TEM)

Two different methods were used for preparing TEM samples. Samples for cross-sectional viewing were prepared by mounting broken fragments of the membrane/support structure onto fused silica cylinders such that the membrane layer was adjacent to the fused silica surface. These samples were sec-

tioned with a diamond wafering saw, ground and polished to a thickness of about 1 μm , and ion milled to a thickness of several hundred ångströms. Cross-sectional TEM was performed using a Philips Model CM-30 300 kV analytical instrument equipped with a LINK EDS analyzer. Plan-view TEM samples were prepared by scraping the membrane layer with a sharp metal knife onto carbon coated TEM support grids. This method provides plan-view imaging of the membrane through the silicate layer and an uncontrolled thickness of the γ -alumina layer. A JEOL 2000FX instrument equipped with a Tracor-Northern EDS analyzer was used for the plan-view imaging.

Ellipsometry

Thickness and refractive index of the companion thin film samples deposited on silicon wafers were measured using a Rudolph Model AUTOELIV ellipsometer by assuming an absorption coefficient of 0.

Transport measurements

Single-gas permeabilities of the uncoated support and coated membranes were measured as a function of pressure using helium and nitrogen. The tubular membrane was supported in a gas flow cell so that compression of viton gasket material at the ends of the membranes prevented bypassing. Compressed pressure-regulated gas at room temperature was flowed into the annulus of the membrane, with the flow-rate set using a mass flow controller, and exited at the outside of the membrane. The pressure drop across the membrane was measured using pressure gauges, and the average pressure across the membrane could be varied using a valve downstream from the flow cell. The methodology employed for the permeability measurements was as follows. Membranes or supports were loaded into the flow cell and outgassed at approximately 150°C for 8 h with a continual helium flow of ca. 10 cm^3/min . The flow cell and membrane were then allowed to cool to room temperature before beginning the permeability measurement. The permeability measurements were then conducted by measuring the pressure on both sides of the membrane as a function of the steady-state mass flow-rate permeating the membrane.

RESULTS AND DISCUSSION

Membrane characteristics

When preparing a membrane by slip-casting or dip-coating from a polymeric sol, the pore size and pore volume depend [20] on the structure of the inorganic polymers (e.g. size and mass fractal dimension), the reactivity of these species (e.g. the condensation or aggregation rates), the time scale of the deposition process (related to the casting time, substrate withdrawal rate, and film thickness), and the magnitude of the shear forces and capillary forces that accom-

pany membrane deposition (related to the surface tension of the solvent and possible surface tension gradients in mixed solvents). See Fig. 5.

One strategy for the preparation of ultramicroporous membranes from polymeric sols relies on the concept of mutual transparency or opacity of fractal clusters. Mandelbrot [22] has shown that if two structures of radius r_c and mass fractal dimensions D_1 and D_2 are placed independently in the same region of space, the mean number of intersections $M_{1,2}$ is expressed as

$$M_{1,2} \propto r_c^{D_1+D_2-d} \quad (1)$$

where d is the dimension of space. Thus, in three dimensions, if each structure has a fractal dimension D less than 1.5, the probability of intersection decreases indefinitely as r_c increases. These structures are mutually transparent: during membrane formation they should freely interpenetrate one another as they are forced into close proximity first by the increasing concentration and then by capillary forces accompanying drying (see Fig. 5). This situation should

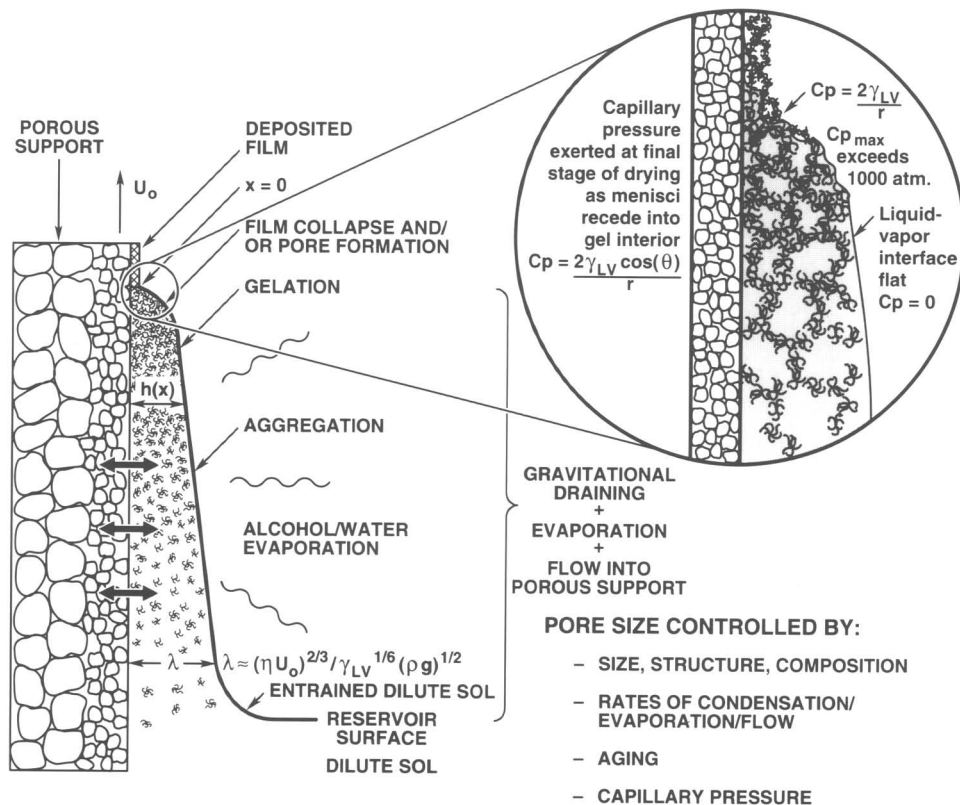


Fig. 5. Physical and chemical processes which occur during membrane preparation by dip coating/casting, and which determine pore size of the membrane.

yield very small pore sizes. SAXS analysis of the sol prior to film deposition indicated a Guinier radius of the silicate polymers $R_G \approx 17 \text{ \AA}$ and a mass fractal dimension $D \approx 1.23$, satisfying the conditions for mutual transparency. In addition, the sol was deposited under acidic conditions where the polymerization rate should be nearly minimized. This too promotes polymer interpenetration and small pore sizes.

Cross-sectional TEM analysis showed the membrane layer to be featureless at magnifications of 1 Mx, consistent with an ultramicroporous texture. A sharp membrane/support interface was observed although EDS analysis indicated minor amounts of silicon in the support to depths of less than 1000 Å. See section *Structural characterization of catalytic membranes* and ref. 21. Based on X-ray fluorescence (XRF), TEM [21] and ellipsometry measurements the thickness of the deposited membranes was estimated to be ca. 1000 Å. These observations are consistent with the results reported by Uhlhorn et al. [23,24]. Utilizing similar supports and silica membrane preparation, they estimated the silica layer to be 300–600 Å. However, comparison with their work is very difficult because a single-step hydrolysis procedure was used for sol preparation, rather than the two step procedure used here. Even with the two-step procedure, relatively subtle changes in conditions, such as pH, can dramatically effect the sol characteristics, support penetration, and membrane properties [21]. The pore diameter of the deposited silica layer, though not yet definitively determined, was estimated to be less than 10 Å based on permeability measurement and analysis, and sorption measurements of films on dense substrates made using a surface acoustic wave (SAW) device [21].

Ellipsometry of companion samples deposited on silicon by dip coating indicate a film thickness of 1250 Å and refractive index of 1.435. If we assume the siloxane skeleton to have refractive index identical to fused silica (ca. 1.45), this refractive index is consistent with a porosity of <5% according to the Lorentz-Lorenz analysis [20]. Most likely the refractive index of the hydroxyl terminated siloxane skeleton exceeds 1.45, so the actual porosity is probably $\geq 5\%$. Though the properties of a membrane layer deposited on a porous support cannot generally be assumed to be the same as films deposited on dense substrates [20] due in part to different time scales of the deposition processes, the fact that the sols were prepared under conditions where the condensation rate is nearly minimized should minimize differences between the membranes and companion films [25,26], and thus should provide a reasonable estimate of the membrane properties, as well as a check on the sol properties.

Transport characteristics of catalytic membranes

Single-gas permeability measurements were carried out at room temperature on the support after each step of the catalytic membrane preparation (deposition, silylation, reduction) to determine the effects of the preparation on pore size reduction or pore plugging. The permeation data are reported in units

of $\text{cm}^3/\text{cm}^2 \text{ s cm Hg}$ (which we call “permeance”), rather than Barrer units ($1 \text{ Barrer} = 10^{-10} \text{ cm}^3 \text{ cm}/\text{cm}^2 \text{ s cm Hg}$), because the appropriate layer thickness to apply is unclear in such a composite structure. The reported units thus represent the flux arising due to the total transport resistance offered by the support plus coating(s). One coating of the membrane prepared from an A2 sol (10 h aging, 2:1 dilution, 100 s dipping time) caused a reduction in permeation rate by about 80% for both helium and nitrogen. The helium and nitrogen permeances were essentially independent of pressure before and after the membrane layer deposition, indicating Knudsen-like transport behavior (Fig. 6). The He/N_2 ideal selectivities before and after membrane coating were 1.6 and 1.4, respectively. These values are below ideal Knudsen values because of the elevated downstream pressure, and also perhaps due to nitrogen surface diffusion.

Upon silylation and drying of the above membrane a further reduction in the helium permeance of about 15% was found to occur (Fig. 6). The He/N_2 selectivity changed from 1.4 to 1.3, a difference which is not significant. The reduction in permeance with silylation could be explained in several ways: (1) an effective reduction in average pore size due to incorporation/reaction of the silylating agent on pore walls, (2) partial pore blockage by the silylation compound or organic products derived from it, or (3) since methanol was used as a solvent for the silylation reaction, esterification of the silanol groups and siloxane bond alcoholysis [20] could have occurred as observed during the aging of bulk, wet silica gels in various fluids [27].

Reaction with $[(1,5\text{-COD}) \text{RhCl}]_2$ and subsequent hydrogen reduction caused the permeance to drop further by about 40% (Fig. 6). A negligible change in He/N_2 selectivity occurred after metal dispersion. The permeance reduction

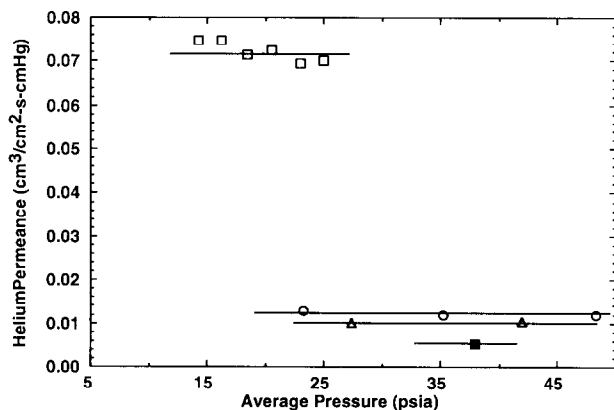


Fig. 6. Helium permeance of the membrane for each of the processing steps of the silylation- $[(1,5\text{-COD}) \text{RhCl}]_2$ reaction approach. (□) Support, (○) support + membrane, (△) after silylation, (■) after metal reduction.

was probably due to partial blockage of pores or pore size reduction caused by the metal particles and/or by deposition resulting from the silylation treatment. Because of the size of the ligands, the $[(\text{COD})\text{RhCl}]_2$ precursor, which has a maximum dimension of ca. 10 Å, was not expected to penetrate the ultramicroporous separation layer to a great extent (TEM observations discussed in the next section verified that rhodium was only deposited on the surface). Therefore, any incompletely removed organic material derived from the metal precursor was most likely confined to the membrane surface and should not have contributed significantly to the reduced permeability.

Permeation measurements were also made at each stage of the $\text{Rh}(\text{acac})_3$ impregnation approach. Helium permeance decreased dramatically following the $\text{Rh}(\text{acac})_3$ impregnation, THF wash and calcination at 200°C in air (Fig. 7). This was probably due to partial pore blockage or pore size reduction resulting from undecomposed or partially decomposed $\text{Rh}(\text{acac})_3$, or to metal/metal oxide decomposition products within the pores. TGA measurements in air and oxygen revealed no significant decomposition of $\text{Rh}(\text{acac})_3$ until ca. 250°C. However, some decomposition may have occurred during the long period of the calcination. Following the metal reduction step the permeance increased to a level higher than the untreated membrane, and showed a pressure dependence indicative of viscous flow. These results suggest that volatiles produced by the reduction of $\text{Rh}(\text{acac})_3$ located within the pores generate defects with pore sizes large enough to support viscous flow (i.e. pore size \gg gas mean free path). The silylation approach, in contrast, apparently prevented the metal-organic precursor from entering the pores, thus avoiding disruption of the membrane layer during decomposition of the metal-organic precursor.

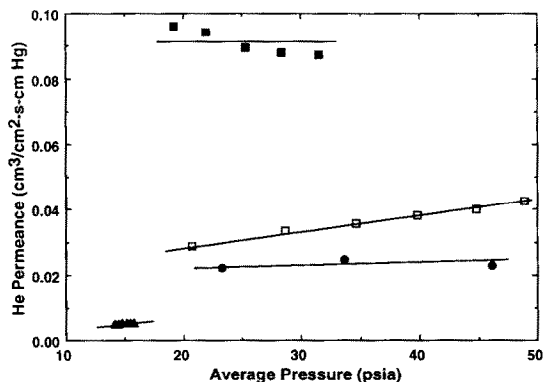


Fig. 7. Helium permeance of the membrane for each of the processing steps of the $\text{Rh}(\text{acac})_3$ impregnation reaction approach. (■) Support, (●) support + membrane, (▲) after metal impregnation + calcining, (□) after reduction.

Structural characterization of catalytic membranes

Cross-sectional TEM of the sample prepared using silylation with the [(1,5-COD) RhCl]₂ precursor (Fig. 8) revealed that the rhodium particles were dispersed exclusively at the surface of the silicate layer. It is likely that the particles were trapped at the surface of the membrane because the precursor molecules were too large to penetrate the small tortuous pores of the silylated silica layer. Work is presently underway to determine whether the Rh(acac)₃ preparation technique also traps the rhodium particles at the surface of the membrane, or whether that precursor is able to penetrate the ultramicroporous layer (cross-sectional TEM has not yet been obtained for the Rh(acac)₃ treated membrane).

Figs. 9a and b show dark-field images from the plan-view TEM samples. Fig. 9a shows the sample derived from surface-confined [(COD) RhCl]₂, and Fig. 9b shows the Rh(acac)₃-derived sample. In both cases, the rhodium particles, seen as light particles against a dark background, are well dispersed throughout the sample. The sample derived from surface-confined [(COD) RhCl]₂ contains more rhodium particles with an average particle size of ca. 6 nm. The Rh(acac)₃-prepared sample contains fewer rhodium particles of a smaller size



Fig. 8. Cross-sectional TEM image of rhodium particles attached to surface of porous SiO₂ layer on γ -Al₂O₃ membrane support prepared by the silylation-[(1,5-COD) RhCl]₂ reaction approach. Region A indicates γ -Al₂O₃ support layer, B indicates porous SiO₂ layer, and C indicates layer of rhodium particles.

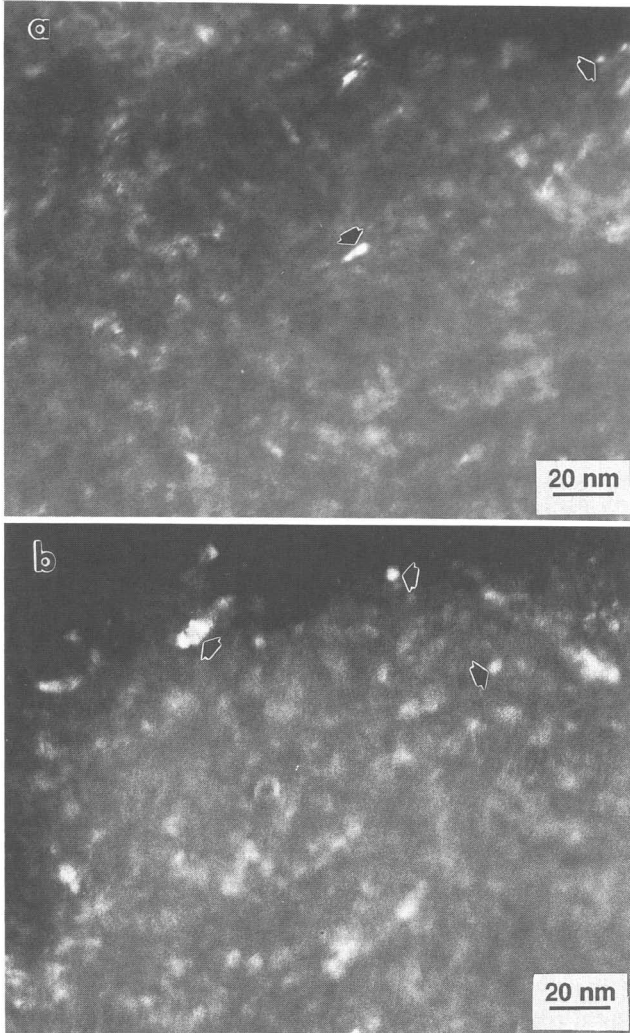


Fig. 9. Plan-view TEM image of rhodium particles on porous SiO_2 layer on $\gamma\text{-Al}_2\text{O}_3$ membrane support. Arrows indicate rhodium particles. (a) Prepared by $\text{Rh}(\text{acac})_3$ impregnation method. (b) Prepared by the silylation- $[(1,5\text{-COD})\text{RhCl}]_2$ reaction method.

(average size ca. 4 nm). EDS spectra from the two plan-view samples indicated that there was approximately 60% more rhodium per mass of silicon in the $[(\text{COD})\text{RhCl}]_2$ sample than in the $\text{Rh}(\text{acac})_3$ sample, as measured by peak intensities of the K_a energies. Since the strength of the interaction of $\text{Rh}(\text{acac})_3$ with the silanol surface is much less than that of $[(\text{COD})\text{RhCl}]_2$ with the silylated surface, the THF wash procedure probably removed most of the surface $\text{Rh}(\text{acac})_3$ leaving only $\text{Rh}(\text{acac})_3$ that had penetrated the pores. This

explains the lower surface coverage and slightly reduced particle size using the $\text{Rh}(\text{acac})_3$ approach. Use of a higher $\text{Rh}(\text{acac})_3$ concentration without the THF wash led to slightly larger particles and a higher particle loading.

SUMMARY AND CONCLUSIONS

From the standpoint of preparing an attractive catalytic membrane, it is desirable to achieve a high catalytic surface area without a detrimental impact of the catalyst dispersion technique on the membrane permselectivity. Two approaches utilizing metal-organic precursors were utilized to disperse rhodium metal particles onto an ultramicroporous silica membrane. One approach involved reaction of membrane surface silanols with a silylating agent [$\text{H}_2\text{N}(\text{CH}_2)_2\text{NH}(\text{CH}_2)_3\text{Si}(\text{OCH}_3)_3$] to provide reactive sites to complex the metal-organic precursor [(1,5-COD) $\text{RhCl}]_2$, followed by reduction in hydrogen. The second approach involved impregnation of a metal-organic precursor [$\text{Rh}(\text{acac})_3$] solution into the microporous support, followed by air calcination and hydrogen reduction. The silylation/metal-organic reaction approach led to a high coverage of nm-sized rhodium particles which were confined to a discrete layer on the surface of the membrane. Apparently, the large size of the [(1,5-COD) $\text{RhCl}]_2$, coupled with pore size reduction due to silylation, prevented significant penetration of the precursor into the pores of the membrane layer. This approach led to a controllable dispersion of rhodium on the surface of the membrane with no disruption of the membrane during the precursor decomposition. In addition, the reduced metal was dispersed using a relatively low-temperature (200°C) reduction, which may have advantages with respect to membrane stability compared to techniques which require higher temperature oxidative heat treatments. A modest reduction in membrane permeability (ca. 40%) occurred, probably due to pore size reduction resulting from silylation or partial pore blockage by rhodium particles.

With the $\text{Rh}(\text{acac})_3$ approach, there is less control of metal loading, dispersion, and location. Since the interaction of $\text{Rh}(\text{acac})_3$ with the surface silanols is much less strong than [(1,5-COD) $\text{RhCl}]_2$ with the silylation agent, the $\text{Rh}(\text{acac})_3$ treatment resulted in lower surface coverage of metal and the metal is not as effectively constrained to a surface layer. Though the $\text{Rh}(\text{acac})_3$ molecule is comparable in size to that of [(1,5-COD) $\text{RhCl}]_2$, $\text{Rh}(\text{acac})_3$ is apparently able to penetrate into the non-silylated ultramicroporous layer due to the larger pore size and a reduced "capture" efficiency. This ultimately leads to disruption of the membrane layer due to decomposition products evolved during the reduction step.

ACKNOWLEDGEMENTS

Portions of the work were supported by the Electric Power Research Institute and National Science Foundation, and by the Gas Research Institute. In

addition, we are grateful to T. Tribble of Sandia National Laboratories for the cross-sectional TEM sample preparation and analysis, and R.G. Tissot of Sandia National Laboratories for the X-ray micro fluorescence. Portions of the TEM work were completed in the Electron Microbeam Analysis Facility in the Department of Geology and Institute of Meteoritics at the University of New Mexico. Sandia National Laboratories is a US Department of Energy facility supported by DOE Contract Number DE-AC04-76-DP00789.

REFERENCES

- 1 J.F. Roth, in J.W. Ward (Editor), *Catalysis 1987 (Studies in Surface Science and Catalysis, Vol. 38)*, Elsevier, Amsterdam, 1988, p. 925.
- 2 N. Itoh, Y. Shindo, K. Haraya and T. Hakuta, *J. Chem. Eng. Jpn.*, 21 (1988) 399.
- 3 Y.M. Sun and S.J. Khang, *Ind. Eng. Chem. Res.*, 27 (1988) 1136.
- 4 V.M. Gryaznov, V.S. Smirnov and M.G. Slin'ko, *Proc. 5th International Congress on Catalysis, Vol. 2, 1973*, p. 1139.
- 5 H.P. Hsieh, *Catal. Rev.-Sci. Eng.*, 33 (1,2) (1991) 1-70.
- 6 V.T. Zaspalis and A.J. Burggraaf, in R.R. Bhave (Editor), *Inorganic Membrane Synthesis, Characteristics and Applications*, Van Nostrand Reinhold, New York, 1991, p. 177.
- 7 M.P. Harold, P. Cini, B. Patenaude and K. Venkataraman, *AIChE Symp. Ser.*, 85(268) (1989) 26.
- 8 V.T. Zaspalis, W. van Praag, K. Keizer, J.G. van Ommen, J.R.H. Ross and A.J. Burggraaf, *Appl. Catal.*, 74 (1991) 235-248.
- 9 D. Eng and M. Stoukides, *Catal. Rev. - Sci. Eng.*, 33(3,4) (1991) 375-412.
- 10 A.G. Anshits, A.N. Shigapov, S.N. Vereshchagin and V.N. Shevnin, *Catal. Today*, 6 (1990) 593-600.
- 11 Y. Liu, A.G. Dixon, Y.H. Ma and W.R. Moser, *Sep. Sci. Technol.*, 25(13-15) (1990) 1511-1521.
- 12 A.M. Champagnie, T.T. Tsotsis, R.G. Minet and I.A. Webster, *Chem. Eng. Sci.*, 45(8) (1990) 2423-2429.
- 13 R.J.R. Uhlhorn, K. Keizer and A.J. Burggraaf, *J. Membr. Sci.*, 46 (1989) 225-241.
- 14 K. Keizer, R.J.R. Uhlhorn, R.J. Van Vuren and A.J. Burggraaf, *J. Membr. Sci.*, 39 (1988) 285-300.
- 15 V.T. Zaspalis, W. van Praag, K. Keizer, J.G. van Ommen, J.R.H. Ross and A.J. Burggraaf, *Appl. Catal.*, 74 (1991) 249-260.
- 16 J.G. van Ommen, H. Boach, P.J. Gellings and J.R.H. Ross, in B. Delmon, P. Grange, P.A. Jacobs and G. Poncelet (Editors), *Preparation of Catalysts IV (Studies in Surface Science and Catalysis, Vol. 31)*, Elsevier, Amsterdam, 1987, p. 151.
- 17 F. Rousseau, Z. Duan, M.J. Hampden-Smith and A. Datye, in M. Hampden-Smith, W. Klemperer and C.J. Brinker (Editors), *Better Ceramics Through Chemistry*, Mater. Res. Soc., Pittsburgh, 1992, in press.
- 18 B. Breitscheidel, J. Zieder and U. Schubert, *Chem. Mater.*, 3 (1991) 559-566.
- 19 J.R. Miller and W.J. Koros, *Sep. Sci. Technol.*, 25(13-15) (1990) 1257-1280.
- 20 C.J. Brinker and G.W. Scherer, *Sol-gel Science*, Academic Press, San Diego, 1990, pp. 185-191.
- 21 C.J. Brinker, T.L. Ward, R. Sehgal, N.K. Raman, S.L. Hietala, D.M. Smith, D.-W. Hua and T.J. Headley, *J. Membr. Sci.*, (1992), submitted for publication.
- 22 B.B. Mandelbrot, *The Fractal Geometry of Nature*, Freeman, San Francisco, 1982.

- 23 R.J.R. Uhlhorn, M.H.B.J. Huis In't Veld, K. Keizer, A.J. Burggraaf, *J. Mater. Sci. Lett.*, 8 (1989) 1135-1138.
- 24 R.J.R. Uhlhorn, K. Keizer and A.J. Burggraaf, *J. Membr. Sci.*, 66 (1992) 271-287.
- 25 C.J. Brinker, A.J. Hurd, G.C. Frye, T.R. Schunk and C.S. Ashley, *J. Ceram. Soc. Jpn.*, 99 (1991) 862-877.
- 26 C.J. Brinker, G.C. Frye, A.J. Hurd and C.S. Ashley, *Solid Films*, 201 (1991) 97-108.
- 27 P.J. Davis, C.J. Brinker and D.M. Smith, *J. Non-Cryst. Solids*, (1991), in press.